A simulation investigation of barium phosphate glasses enhanced with vanadium and tellurium ions for X- and gamma energies attenuation

M. M. Damoom [a,b], A.M. Alhawsawi [a,b], E.B. Moustafa [c], A. H. Hammad [d,*]
[a] *Nuclear Engineering Department, Faculty of Engineering, King Abdulaziz University, P.O. Box 80204, 21589 Jeddah, Saudi Arabia.*
[b] *Center for Training & Radiation Prevention, King Abdulaziz University, P.O. Box 80204, Jeddah, 21589, Saudi Arabia.*
[c] *Mechanical Engineering Department, Faculty of Engineering, King Abdulaziz University, P.O. Box 80204, 21589 Jeddah, Saudi Arabia.*
[d] *Center of Nanotechnology, King Abdulaziz University, Jeddah 21589, Saudi Arabia*

Barium phosphate glass with fixed barium oxide (BaO) at 40 mol% and vanadium oxide (V_2O_5) at 1 mol% was successfully synthesized by the melt quenching process. Different concentrations of tellurium oxide (TeO_2) were introduced at the expense of the phosphate groups (P_2O_5) to improve and modify the elastic and radiation shielding properties. The elastic parameters were calculated from the Makishima-Mackenzie model. The radiation shielding parameters were simulated and studied using the XCOM database to check the availability of such glass to withstand the X-ray and gamma energies.

(Received July 8, 2024; Accepted September 27, 2024)

Keywords: Phosphate, Tellurium ions, Elastic parameters, Radiation shielding, Monte Carlo simulation

1. Introduction

The phosphate (P_2O_5) network is a typical type of glass that looks silicate (SiO_2), borate (B_2O_3), and germanate (GeO_2). The tetrahedral structural PO_4 units, in which the phosphorous atom forms a singly bond with four oxygen atoms, explain the physical and chemical features of the phosphate network. Besides, a double bond develops between the phosphorous atom and the last oxygen atom. Consequently, the P_2O_5 ratio in the glass network determines the different modes of the PO_4 units [1, 2]. The Q^n model characterizes these modes when n, the number of bridging oxygens in the structural units, is equal 0, 1, 2, or 3 [1].

When used as a glass modifier, the addition of Ba ions to the glass lowered both the glass transition and the melting glass point (BaO_6 units). Moreover, the high BaO content in glass shows as BaO_4 units, thus it might also be used as a glass former. Barium ions improve the ionic conductivity [3, 4], luminous efficiency [5], radiation shielding [6], and elasticity properties [7, 8]. TeO_2 is another material used to form conditional glass networks. The TeO_2 compound is made up of TeO_4 trigonal bipyramids, with one of the equatorial sites occupied by a single pair of electrons [9, 10]. With a high TeO_2 content, these units exhibit a nearly distorted mode, suggesting TeO_3 trigonal pyramids. Therefore, the radiation shielding protection can be enhanced by the high bulk density of TeO_2 (5.67 g/cm^3).

The effect of TeO_2 additions on the elastic and radiation shielding characteristics of glasses composed of 49% BaO, 59% P_2O_5, and 1% V_2O_5 is addressed in this work. The elastic and shielding properties were computed by the empirical Makishima-Mackenzie model and XCOM simulation, respectively. This research is expected to produce good elastic, nontoxic glass with excellent radiation shielding properties.

* Corresponding author: ahhhassan@kau.edu.sa
https://doi.org/10.15251/JOR.2024.205.681

2. Experimental and simulation details

2.1. The glass preparation and density measurements

The current study focuses on the composition (mol%) of 40BaO–1V_2O_5–(59-*x*)P_2O_5–*x*TeO_2, which was synthesized through the melt-quenching process. The range of *x* is 0 to 20 mol%, with a 5% step. The glass was made with high-purity (99%) chemicals such as $BaCO_3$, V_2O_5, $NH_4H_2PO_4$, and TeO_2. Table 1 shows the current glass compositions and labels. The selected chemicals' powders were weighed and placed in porcelain crucibles before being melted in an electrical furnace at 1200 °C Celsius for 90 minutes. The crucibles were shaken three times to ensure melt homogeneity. The melt was then distributed into specific shapes in the graphite mold, which was heated to 350 °C and allowed to cool to room temperature.

The density of the glass was determined by applying the Archimedes principle, which involved weighing the sample in air and then immersing it in a stable liquid, such as xylene (ρ_{exp} = 0.863 g/cm^3).

Table 1. The component of the glass in mol%, and their densities in g/cm^3.

Glass Label	TeO_2	P_2O_5	BaO	V_2O_5	ρ_{exp}
0TeO_2	0	59	40	1	3.263
5TeO_2	5	54	40	1	3.238
10TeO_2	10	49	40	1	3.173
15TeO_2	15	44	40	1	3.046
20TeO_2	20	39	40	1	3.486

2.2. The elastic parameters' calculations

The elastic parameters of such glasses are predicted from the glass composition and density using the Makishima-Mackenzie model [11, 12]. These parameters include Yong's modulus (*Y*), bulk modulus (*B*), shear modulus (*S*), Poisson's ratio (*P*), and hardness number (H_v) [13, 14], which depends on the ionic packing ratio (V_P). The V_p is correlated to the values of ρ_{exp} by the Inaba-Fujino (*I-F*) empirical formula [15].

$$\frac{V_P}{\rho_{exp}} = \frac{\Sigma V_i x_i}{\Sigma M_i x_i} \tag{1}$$

The term V_i represents the packing density of each oxide (A_aO_o) in the glass composition, while $\Sigma M_i x_i$ represents the molecular weight of the glass. Therefore, the following equations are used to calculate the elastic parameters with the help of the dissociation energy per unit volume (G_i):

$$Y = 8.36\ \Sigma G_i x_i \tag{2}$$

$$B = 10 V_P^2\ \Sigma G_i x_i \tag{3}$$

$$S = \frac{10 V_P^2}{10.2 V_P - 1}\ \Sigma G_i x_i \tag{4}$$

$$P = \frac{1}{2} - \frac{1}{7.2 V_P} \tag{5}$$

$$H_v = \frac{E(1-2P)}{6(1+P)} \tag{6}$$

2.3. Monte Carlo radiation shielding simulation

XCOM, or the Photon Cross Sections Database, is the database that is most frequently used to compute the mass attenuation coefficients (μ_m) [16, 17]. XCOM takes into account all possible interactions between the material and photons, computationally determines the total mass attenuation coefficients of any element, compound, or mixture from 1 keV to 100 GeV.

The program provides pair production attenuation coefficients, photoelectric absorption, coherent and incoherent scattering, and more. The total of these interaction coefficients is the computed total attenuation coefficient [18]. When predicting the total attenuation coefficients of composite materials, like glass, the XCOM program needs to know the weight fraction of each component.

The average number of photon-matter interactions in a given mass per unit area of the encountered material is taken into account by the μ_m [19]. The glass's μ_m is then obtained from the XCOM database, and the following equations [20-23] are used to compute the other radiation shielding parameters:

$$\mu\ (cm^{-1}) = \mu_m \times \rho_{exp} \tag{7}$$

$$MFP\ (cm) = 1/\mu \tag{8}$$

$$HVL\ (cm) = ln(2) \times MFP \tag{9}$$

$$TVL\ (cm) = ln(10) \times MFP \tag{10}$$

$$Z_{eff} = \frac{\sigma_a}{\sigma_e} = \frac{\frac{1}{N_A}\sum f_i A_i (\mu_m)_i}{\frac{1}{N_A}\sum \frac{f_i A_i (\mu_m)_i}{Z_i}} \tag{11}$$

Hence, the linear attenuation coefficient (μ), mean free path (*MFP*), half and tenth value layers (*HVL* and *TVL*), and effective atomic number (Z_{eff}) are the radiation parameters computed from the μ_m. The connections between these different parameters are shown by the equations from (7) to (11). Avogadro's number is denoted by N_A, the effective atomic cross section by σ_a, the electronic cross section by σ_e, the atomic weight and atomic number of an element *i* by A_i and Z_i, and the fraction of element *i* by f_i.

3. Results and discussion

3.1. The elastic properties

When an external load is applied, a material's ability to withstand or resist deformation is defined by its elastic parameters. The *E*, *B*, *S*, *P*, and H_v parameters are these ones. The relationship between the TeO_2 content and the elastic parameters *E*, *B*, and *S* is displayed in Fig. 1. The $15TeO_2$ sample showed a low *E* value of 49.216 GPa, while the free glass sample had a high Young's modulus of 62.317 GPa. It was found that the E values dropped when the TeO_2 content was intercalated from 20 mol% to 53.087 GPa. As seen in Fig. 1, the same patterns were noted for the *B* and *S* for different glasses. Therefore, the $0TeO_2$ sample exhibited better elastic properties than the glasses containing TeO_2. Fig. 2 illustrates the behavior of the Poisson's ratio and the hardness number. The *P* values decrease with an increase in TeO_2 content, from 0.259 to 0.227, where TeO_2 varies from 0 to 20 mol%. The H_v trend increases as the TeO_2 increases from 3.962 GPa to 4.047 GPa, where TeO_2 varies from 0 to 15 mol%, but there is a slight decrease at the high TeO_2 content (20 mol%) to 3.936 GPa. Therefore, the presence of TeO_2 improves the glass hardness, especially in the sample, which contains 15 mol%.

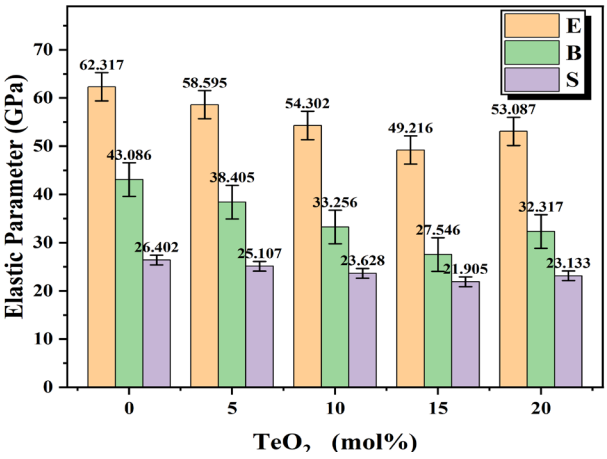

Fig. 1. The variation of the elastic parameters E, B, and S for different glasses.

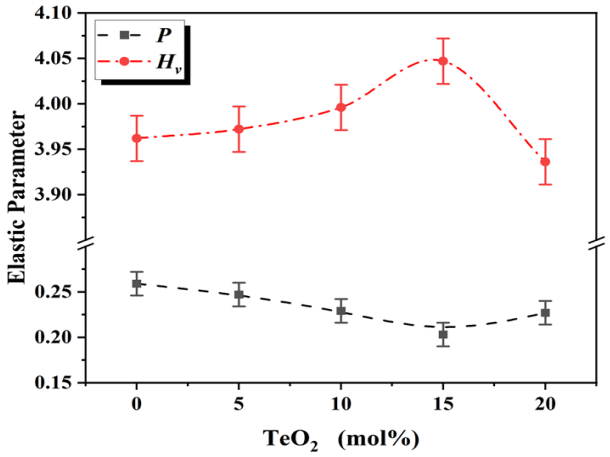

Fig. 2. The P and H_v vs. TeO_2 content.

3.2. The radiation shielding properties

Fig. 3 (a) illustrates the μ_m of barium vanado-phosphate glass with varying concentrations of tellurium oxide. This study examines the radiation shielding properties in relation to the simulation of X-ray radiation and various significant gamma-ray energies. Therefore, the energy of the radiation increases from 5.888 keV to 2.506 MeV. The current glasses effectively reduce low-energy radiation and X-ray radiation. In the case of low-energy radiation at 5.888 keV, the μ_m for the base or the $0TeO_2$ sample measured 293.968 cm^2/g, while it increased to 371.913 cm^2/g for the glass containing 20% TeO_2. The X-ray characteristics zone spans from 8.04 keV for Cu K_α to 50.38 keV for Tb K_β. Thus, the μ_m value of the $0TeO_2$ glass decreased significantly from 147.614 to 5.263 cm^2/g. Similarly, the glass with a higher tellurium content of 20% also experienced a decrease in μ_m value from 182.444 cm^2/g to 6.990 cm^2/g. TeO_2 enhances the μ_m of the glass under X-ray radiation. For high-energy radiation, the energy ranges from 59.54 keV to 2.506 MeV. The μ_m decreased from 3.413 to 0.038 cm^2/g for the $0TeO_2$ sample. The glass containing 20% TeO_2 had a higher μ_m than the base sample at 59.54 keV, which was raised to 4.511 cm^2/g. However, the μ_m value stays constant at 2.506 MeV, as shown in Table 2. In general, the μ_m values depend on the exponent of the radiation energy, and the μ_m is inversely proportional to the energy exponent of -3.5 in the photoelectric effect (*PE*) region from 1 to 100 keV, while it is proportional to the energy exponent of -1 in the compton scattering (*CS*) region from 100 keV to 12 MeV [13, 24-27], as shown in Fig. 3(b) and Fig. 3(c). The current μ_m values of 0.6617, 1.173, and 1.333 are similar and close to those reported in previous published research for Li_2O-BaO-Bi_2O_3-P_2O_5 and TeO_2-ZnO-Na_2O glass systems [6, 28].

Similarly, the linear attenuation coefficient (μ) is directly proportional to the μ_m when multiplied with the glass density (D), as shown in equation (7). The values of μ are essential for calculating the other radiation shielding parameters, especially the *MFP*, *HVL*, and *TVL*. Table 3 shows the *MFP* values for the current samples. *MFP* refers to the mean free path of atoms, molecules, or photons before they experience significant changes in their direction, energy, or other properties.

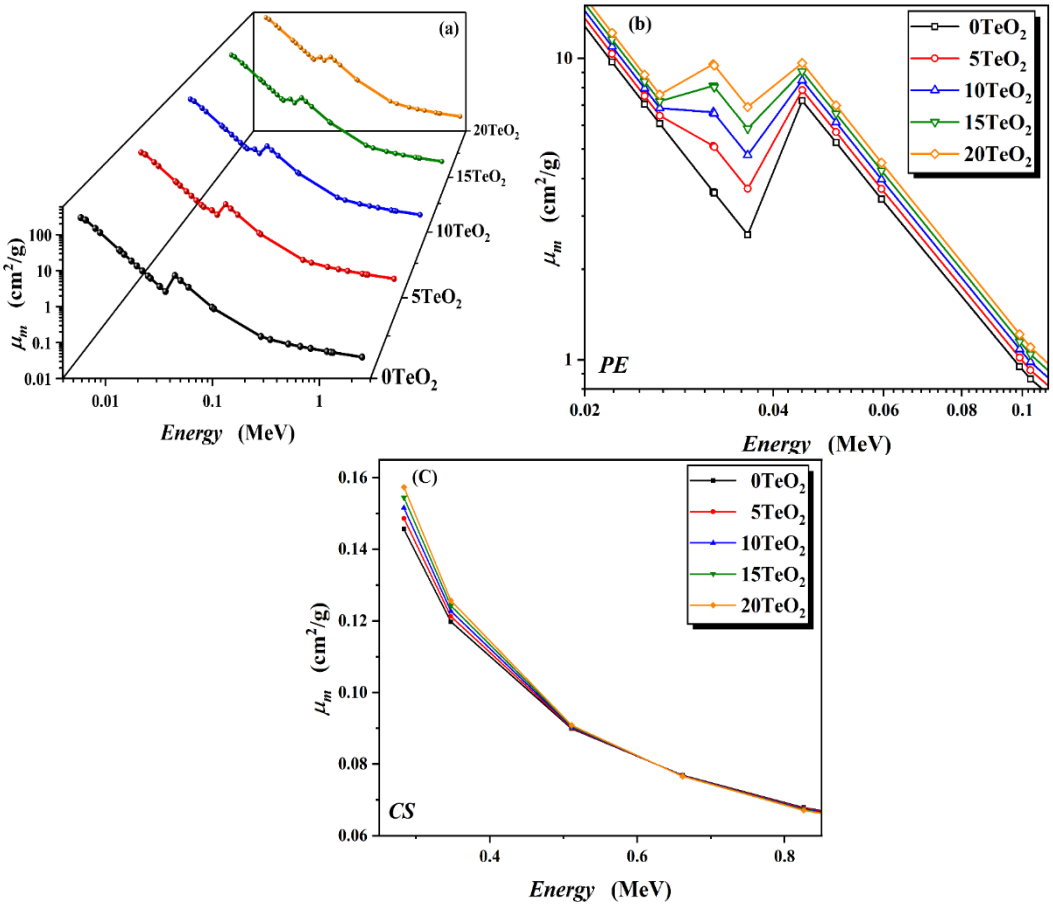

Fig. 3. (a) The behavior of the μ_m at different radiation energies for different glass compositions; (b) The variation of the μ_m in the PE region; and (c) in the CS region.

For X-ray energies, the *MFP* had 0.582 ml at 50.38 keV, which decreased to 0.41 ml for $0TeO_2$ and 20 TeO_2, respectively. These values increased with gamma energies, as shown in Table 2. For example, the *MFP* at 661 keV was 3.9888 cm for $0TeO_2$, which was reduced to 3.74 cm when TeO_2 participated with 20% of the glass component. These values reflect the *HVL* and *TVL* characteristics, as shown in equations (8, 9, and 10).

Figure 4 depicts the *HVL* and *TVL* characteristics. For the $0TeO_2$ sample, a thin 14 μm glass layer can prevent 50% of the X-ray radiation intensity at 8.04 keV. Furthermore, the *HVL* for the $20TeO_2$ sample is 11 μm, which reduces the same radiation intensity. For the same samples, the *TVLs* are 48 and 36 μm, respectively. This means that a small layer of the current glasses could actively shield the X-ray characteristics and reduce the intensity to its half or tenth value. For the gamma radiation energy, which ranges from 59.54 keV to 2.506 MeV, the *HVL* and *TVL* thicknesses for the $0TeO_2$ are 0.622 ml to 5.46 cm and 2.06 ml to 18.14 cm, respectively. These values decrease when TeO_2 contributes to the glass network by 20%, from 0.44 ml to 5.15 cm and from 1.46 ml to 17.10 cm, respectively. Therefore, it can be said that such glasses effectively shield all X-ray

radiation and some gamma energies up to 347.1 keV, requiring a thickness of at least 5.9 cm to reduce the intensity to its tenth value.

Table 2. The mass attenuation coefficient values for barium vanado-phosphate glass with different TeO_2 ratios.

Radiation energy (MeV)	μ_m (cm²/g)				
	0TeO₂	**5TeO₂**	**10TeO₂**	**15TeO₂**	**20TeO₂**
0.005888	293.9683	313.8038	333.4036	352.7721	371.9132
0.005899	292.5605	312.3071	331.8191	351.1007	370.1561
0.00649	256.7663	272.0932	287.2380	302.2039	316.9942
0.006536	252.1369	267.1885	282.0613	296.7585	311.2831
0.00804	147.6141	156.4777	165.2361	173.8911	182.4444
0.00891	112.3170	119.1112	125.8247	132.4590	139.0154
0.01337	37.7984	40.1460	42.4658	44.7581	47.0235
0.01381	34.6545	36.8107	38.9413	41.0467	43.1274
0.01497	27.9193	29.6653	31.3907	33.0956	34.7806
0.01744	18.4544	19.6168	20.7654	21.9005	23.0222
0.01963	13.4184	14.2675	15.1066	15.9358	16.7552
0.0221	9.7320	10.3497	10.9601	11.5633	12.1593
0.0249	7.0602	7.5087	7.9518	8.3897	8.8225
0.02634	6.0733	6.4592	6.8405	7.2173	7.5897
0.03206	3.6128	5.1304	6.6300	8.1118	9.5763
0.03218	3.5776	5.0806	6.5658	8.0334	9.4838
0.03639	2.5998	3.6966	4.7804	5.8514	6.9098
0.04448	7.2420	7.8560	8.4628	9.0624	9.6549
0.05038	5.2639	5.7033	6.1375	6.5665	6.9905
0.05954	3.4134	3.6928	3.9688	4.2416	4.5112
0.09897	0.9501	1.0178	1.0848	1.1509	1.2162
0.103	0.8639	0.9244	0.9842	1.0433	1.1017
0.2835	0.1456	0.1486	0.1516	0.1545	0.1574
0.3471	0.1198	0.1213	0.1227	0.1242	0.1257
0.511	0.0899	0.0901	0.0904	0.0906	0.0908
0.6617	0.0768	0.0768	0.0767	0.0766	0.0766
0.8261	0.0678	0.0676	0.0674	0.0672	0.0671
1.173	0.0560	0.0557	0.0555	0.0552	0.0549
1.275	0.0536	0.0533	0.0530	0.0528	0.0525
1.333	0.0523	0.0521	0.0518	0.0516	0.0513
2.506	0.0389	0.0388	0.0387	0.0387	0.0386

The effective atomic number (Z_{eff}) is another crucial parameter in radiation shielding characteristics. Z_{eff} is dependent on the μ_m of each element in the glass composition, as well as the mole and weight fraction of each constituent. The presence of TeO_2 in the phosphate glass improves the value of Z_{eff}, as shown in Fig. 5. As the TeO_2 content increased, the Z_{eff} also increased. At lower energies from 0.5888 to 44 keV, the Z_{eff} varies from 33.75 to 49.4 and from 40.30 to 51.14 for the $0TeO_2$ and $20TeO_2$ samples, respectively. At 44 keV, the Z_{eff} had a maximum value. The curves abruptly decrease from 44 keV to 283.5 keV, resulting in calculated Z_{eff} values of 17.61 and 21.84 for the base and $20TeO_2$ samples, respectively. As shown in Fig. 5, a slight decrease in the Z_{eff} occurs when the gamma radiation energy increases to 2.506 MeV.

Table 3. The MFP values for BaO-V_2O_5-P_2O_5: TeO_2 glasses.

Radiation energy (MeV)	***MFP (cm)***				
	$0TeO_2$	**$5TeO_2$**	**$10TeO_2$**	**$15TeO_2$**	**$20TeO_2$**
0.005888	0.0010	0.0010	0.0009	0.0009	0.0008
0.005899	0.0010	0.0010	0.0009	0.0009	0.0008
0.00649	0.0012	0.0011	0.0011	0.0011	0.0009
0.006536	0.0012	0.0012	0.0011	0.0011	0.0009
0.00804	0.0021	0.0020	0.0019	0.0019	0.0016
0.00891	0.0027	0.0026	0.0025	0.0025	0.0021
0.01337	0.0081	0.0077	0.0074	0.0073	0.0061
0.01381	0.0088	0.0084	0.0081	0.0080	0.0066
0.01497	0.0110	0.0104	0.0100	0.0099	0.0082
0.01744	0.0166	0.0157	0.0152	0.0150	0.0125
0.01963	0.0228	0.0216	0.0209	0.0206	0.0171
0.0221	0.0315	0.0298	0.0288	0.0284	0.0236
0.0249	0.0434	0.0411	0.0396	0.0391	0.0325
0.02634	0.0505	0.0478	0.0461	0.0455	0.0378
0.03206	0.0848	0.0602	0.0475	0.0405	0.0299
0.03218	0.0857	0.0608	0.0480	0.0409	0.0302
0.03639	0.1179	0.0835	0.0659	0.0561	0.0415
0.04448	0.0423	0.0393	0.0372	0.0362	0.0297
0.05038	0.0582	0.0541	0.0514	0.0500	0.0410
0.05954	0.0898	0.0836	0.0794	0.0774	0.0636
0.09897	0.3226	0.3034	0.2906	0.2853	0.2358
0.103	0.3548	0.3341	0.3202	0.3147	0.2603
0.2835	2.1044	2.0779	2.0795	2.1253	1.8225
0.3471	2.5592	2.5468	2.5679	2.6433	2.2824
0.511	3.4094	3.4261	3.4875	3.6234	3.1570
0.6617	3.9888	4.0227	4.1094	4.2844	3.7459
0.8261	4.5185	4.5660	4.6735	4.8821	4.2767
1.173	5.4749	5.5426	5.6834	5.9478	5.2196
1.275	5.7231	5.7949	5.9432	6.2208	5.4602
1.333	5.8581	5.9319	6.0841	6.3686	5.5902
2.506	7.8803	7.9555	8.1351	8.4900	7.4302

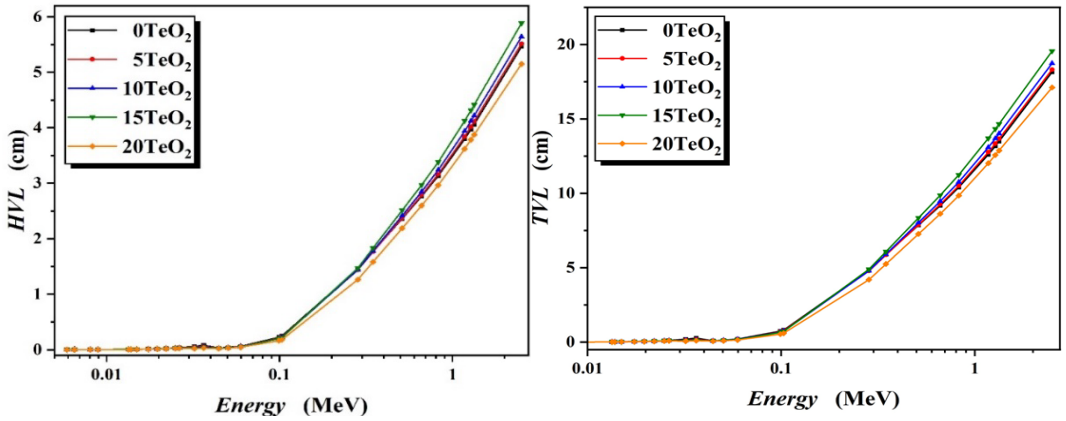

Fig. 4 The HVL and TVL characteristics.

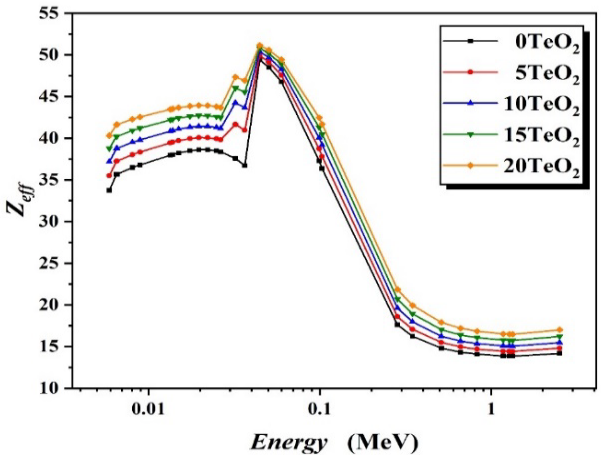

Fig. 5. Z_{eff} vs. radiation energy.

4. Conclusion

The elastic and radiation-shielding properties of barium vanado-phosphate glass containing tellurium oxide are successfully determined using empirical and simulation techniques. The glass with free TeO_2 had higher Young's, bulk, and shear moduli than other glasses with different TeO_2 concentrations. The phosphate glass, which contained 15 mol% of TeO2, had a significantly high hardness value of 4.047 GPa. The inclusion of TeO_2 in the barium phosphate network enhances the radiation shielding properties. With the increase in the TeO_2 content, the mass attenuation coefficient and the effective atomic numer increased, especially in the photoelectric region. In addition, TeO_2 reduces the half- and tenth-value layers. Therefore, such glasses are promising radiation shielding materials for X-rays and some small gamma energies.

Acknowledgements

This research work was funded by Institutional Fund Projects under grant no. (IFPIP: 1688-135-1443). The authors gratefully acknowledge technical and financial support provided by the Ministry of Education and King Abdulaziz University, DSR, Jeddah, Saudi Arabia.

References

[1] J. E. Shelby, Introduction to Glass Science and Technology, second., The Royal Society of Chemistry, Cambridge, UK, (2005).

[2] A. H. Hammad, E. B. Moustafa, and A. R. Wassel, Journal of Materials Research and Technology, 15, 4813 (2021); https://doi.org/10.1016/j.jmrt.2021.10.113

[3] H. Sumi, Y. Nakano, Y. Fujishiro, T. Kasuga, Int J Hydrogen Energy, 38, 15354 (2013); https://doi.org/10.1016/j.ijhydene.2013.09.087

[4] S. H. Lee, S. B. Park, Y. il Park, Solid State Ion, 345, 115186 (2020); https://doi.org/10.1016/j.ssi.2019.115186

[5] Y. Zhuo et al., J Non Cryst Solids, 471, 215 (2017); https://doi.org/10.1016/j.jnoncrysol.2017.05.042

[6] S. Yasmin, M. Kamislioglu, M. I. Sayyed, Optik (Stuttg), 274, 170529 (2023); https://doi.org/10.1016/j.ijleo.2023.170529

[7] Z. Y. Khattari, M. S. Al-Buriahi, Radiation Physics and Chemistry, 195, 110091 (2022); https://doi.org/10.1016/j.radphyschem.2022.110091

[8] M. K. Narayanan, H. D. Shashikala, J Non Cryst Solids, 430, 79 (2015); https://doi.org/10.1016/j.jnoncrysol.2015.10.006

[9] E. F. El Agammy et al., Ceram Int, 46, 18551 (2020); https://doi.org/10.1016/j.ceramint.2020.04.161

[10] N. S. Tagiara et al., J Non Cryst Solids, 457, 116 (2017); https://doi.org/10.1016/j.jnoncrysol.2016.11.033

[11] A. Makishima, J. D. Mackenzie, J Non Cryst Solids, 12, 35 (1973); https://doi.org/10.1016/0022-3093(73)90053-7

[12] A. Makishima, J. D. Mackenzie, J Non Cryst Solids, 17, 147 (1975); https://doi.org/10.1016/0022-3093(75)90047-2

[13] J. Singh et al., Ceram Int, 47, 21730 (2021); https://doi.org/10.1016/j.ceramint.2021.04.188

[14] K. A. Mahmoud, F. I. El-Agawany, O. L. Tashlykov, E. M. Ahmed, Y. S. Rammah, Nuclear Engineering and Technology, 53, 3816 (2021); https://doi.org/10.1016/j.net.2021.06.005

[15] S. Inaba, S. Fujino, Journal of the American Ceramic Society, 93, 217 (2010); https://doi.org/10.1111/j.1551-2916.2009.03363.x

[16] M. J. Berger and J. H. Hubbell, (1987) http://www.osti.gov/servlets/purl/6016002-Jgm0Fa/.

[17] M. J. Berger et al., https://www.nist.gov/pml/xcom-photon-cross-sections-database.

[18] E. Eren Belgin, Radiation Physics and Chemistry, 193, 109960 (2022); https://doi.org/10.1016/j.radphyschem.2022.109960

[19] J. H. Hubbell, Int J Appl Radiat Isot, 33, 1269 (1982); https://doi.org/10.1016/0020-708X(82)90248-4

[20] H. O. Tekin et al., Results Phys, 12, 1797 (2019); https://doi.org/10.1016/j.rinp.2019.02.017

[21] J. H. Hubbell, X-Ray Spectrometry, 28, 215 (1999); https://doi.org/10.1002/(SICI)1097-4539(199907/08)28:4<215::AID-XRS336>3.0.CO;2-5

[22] J. H. Hubbell, Phys Med Biol, 44 (1999); https://doi.org/10.1088/0031-9155/44/1/001

[23] A. Un and T. Caner, Ann Nucl Energy, 65, 158 (2014); https://doi.org/10.1016/j.anucene.2013.10.041

[24] A. M. A. Mostafa, S. A. M. Issa, and M. I. Sayyed, J Alloys Compd, 708, 294 (2017); https://doi.org/10.1016/j.jallcom.2017.02.303

[25] A. B. Chilton, J. K. Shultis, and R. E. Faw, Principles of Radiation Shielding, First., Prentice Hall, New Jercy, (1984).

[26] S. Arivazhagan et al., Radiation Physics and Chemistry, 196, 110108 (2022); https://doi.org/10.1016/j.radphyschem.2022.110108

[27] M. I. Sayyed, S. Hashim, K. G. Mahmoud, A. Kumar, Optik (Stuttg), 274 (2023); https://doi.org/10.1016/j.ijleo.2023.170532

[28] M. S. Al-Buriahi et al., Optik (Stuttg), 257, 168821 (2022); https://doi.org/10.1016/j.ijleo.2022.168821